Arabidopsis RNA Polymerase V Mediates Enhanced Compaction and Silencing of Geminivirus and Transposon Chromatin during Host Recovery from Infection

Tami Coursey,[a,b] Elizabeth Regedanz,[a] David M. Bisaro[a,b]

[a]Department of Molecular Genetics, Center for Applied Plant Sciences, Center for RNA Biology, The Ohio State University, Columbus, Ohio, USA

[b]Graduate Program in Molecular, Cellular, and Developmental Biology, The Ohio State University, Columbus, Ohio, USA

ABSTRACT Plants employ RNA-directed DNA methylation (RdDM) and dimethylation of histone 3 lysine 9 (H3K9me2) to silence geminiviruses and transposable elements (TEs). We previously showed that canonical RdDM (Pol IV-RdDM) involving RNA polymerases IV and V (Pol IV and Pol V) is required for *Arabidopsis thaliana* to recover from infection with *Beet curly top virus* lacking a suppressor protein that inhibits methylation (BCTV *L2⁻*). Recovery, which is characterized by reduced viral DNA levels and symptom remission, allows normal floral development. Here, we used formaldehyde-assisted isolation of regulatory elements (FAIRE) to confirm that >90% of BCTV *L2⁻* chromatin is highly compacted during recovery, and a micrococcal nuclease-chromatin immunoprecipitation assay showed that this is largely due to increased nucleosome occupancy. Physical compaction correlated with augmented cytosine and H3K9 methylation and with reduced viral gene expression. We additionally demonstrated that these phenomena are dependent on Pol V and by extension the Pol IV-RdDM pathway. BCTV *L2⁻* was also used to evaluate the impact of viral infection on host loci, including repressed retrotransposons *Ta3* and *Athila6A*. Remarkably, an unexpected Pol V-dependent hypersuppression of these TEs was observed, resulting in transcript levels even lower than those detected in uninfected plants. Hypersuppression is likely to be especially important for natural recovery from wild-type geminiviruses, as viral L2 and AL2 proteins cause ectopic TE expression. Thus, Pol IV-RdDM targets both viral and TE chromatin during recovery, simultaneously silencing the majority of viral genomes and maintaining host genome integrity by enforcing tighter control of TEs in future reproductive tissues.

IMPORTANCE In plants, RdDM pathways use small RNAs to target cytosine and H3K9 methylation, thereby silencing DNA virus genomes and transposable elements (TEs). Further, Pol IV-RdDM involving Pol IV and Pol V is a key aspect of host defense that can lead to recovery from geminivirus infection. Recovery is characterized by reduced viral DNA levels and symptom remission and thus allows normal floral development. Studies described here demonstrate that the Pol V-dependent enhanced viral DNA and histone methylation observed during recovery result in increased chromatin compaction and suppressed gene expression. In addition, we show that TE-associated chromatin is also targeted for hypersuppression during recovery, such that TE transcripts are reduced below the already low levels seen in uninfected plants. Thus, Pol IV-RdDM at once silences the majority of viral genomes and enforces a tight control over TEs which might otherwise jeopardize genome integrity in future reproductive tissue.

KEYWORDS geminivirus, RNA polymerase V, retrotransposons, Pol V

Address correspondence to David M. Bisaro, bisaro.1@osu.edu.

Most DNA virus genomes are encapsidated free of host nucleosomes and epigenetic modifications but are rapidly converted into nonintegrating minichromosomes upon entry into the host cell nucleus. Conversion is often followed by deposition of repressive histone posttranslational modifications (PTMs) and sometimes also DNA methylation as a host defense that leads to transcriptional gene silencing (TGS). As a counterdefense, viruses encode proteins that, directly or indirectly, reverse or suppress the establishment of repressive modifications and promote productive infection. These early events are a prominent feature of virus-host interactions in several families, including the herpesviruses (1–4) and geminiviruses (5–9).

Plants employ RNA-directed DNA methylation (RdDM) and associated histone 3 lysine 9 dimethylation (H3K9me2) to silence invasive DNAs, including geminivirus genomes and transposable elements (TEs) (10–13). In the model plant *Arabidopsis thaliana*, recent evidence indicates that DNA methylation is initiated at naive TEs and epialleles by expression-dependent mechanisms that involve DNA-dependent RNA polymerase II (Pol II) (14, 15). At these loci, canonical RdDM (Pol IV-RdDM), which involves the plant-specific DNA-dependent RNA polymerases Pol IV and Pol V, plays a key role in reinforcing DNA methylation. In this well-studied pathway, noncoding transcription by Pol IV creates a substrate for RNA-dependent RNA polymerase 2 (RDR2), which generates double-stranded RNA (dsRNA) that is processed by Dicer-like 3 (DCL3) into 24-nucleotide (nt) small interfering RNAs (siRNAs). An siRNA guide strand is incorporated into an Argonaute 4 (AGO4)- or AGO6-containing RNA-induced silencing complex (RISC) and directs RISC by base pairing with a Pol V-generated scaffold transcript that remains associated with the target locus. The tethered RISC then recruits cytosine and histone methyltransferases that write repressive epigenetic marks, which in turn direct remodeling complexes to compact chromatin and create an environment refractory to gene expression. Recent work from our laboratory has confirmed that Pol IV and Pol V are not required to initiate geminivirus DNA methylation but are essential for its amplification. In addition, both are necessary for deposition of H3K9me2 on geminivirus chromatin (16).

Geminiviruses are important pathogens of food and fiber crops that package small circular single-stranded DNA (ssDNA) genomes in unique twin icosahedral particles (17, 18). Viral genomes consist of one or two ~2.5- to 3.0-kb DNAs that are replicated and transcribed by host polymerases and accessory factors. Following nuclear entry, genomic ssDNA is converted into a double-stranded DNA (dsDNA) replicative form (RF) that is bound by histone octamers to form nonintegrating minichromosomes with 11 to 13 nucleosomes (19–21). Reflecting the presence of both repressed and active viral genomes in infected hosts, viral chromatin is decorated with PTMs typical of both repressed and active gene expression (5). Thus, some viral RF DNA is hypermethylated and associated with nucleosomes marked with H3K9me2, while some is hypomethylated and enriched for nucleosomes acetylated at H3K9 and H3K14 (H3K9/14ac) (22, 23). The equilibrium between repressed and active viral chromatin (and thus host defense and viral counterdefense) has a profound impact on the outcome of infection, as a preponderance of the repressed state favors symptom remission and host recovery. Further evidence for viral chromatin methylation as an antiviral defense comes from studies of *Arabidopsis* plants deficient for individual components of the Pol IV-RdDM pathway that leads to chromatin methylation. Specifically, plants lacking Pol IV, Pol V, Classy 1 (CLSY1), DCL3, dsRNA binding 3 (DRB3), or AGO4 exhibit hypersusceptibility and fail to recover from geminivirus infection (5, 16, 22).

While experiments to date have described epigenetic marks present on geminivirus chromatin, relatively little has been done to directly assess the molecular impact of these modifications on chromatin structure and gene expression. One recent report examined viral minichromosomes obtained from symptomatic and recovered nonsymptomatic tissue from pepper plants infected with *Pepper golden mosaic virus* (PepGMV). This study found that most viral chromatin from recovered tissue exists in a highly condensed state, with increased levels of DNA and H3K9 methylation (23).

In the work described here, *Beet curly top virus* (BCTV) and a mutant virus lacking a

silencing suppressor (BCTV *L2⁻*) were used with wild-type and Pol V-deficient *Arabidopsis* plants to examine the link between RdDM and viral chromatin structure. Formaldehyde-assisted isolation of regulatory elements (FAIRE) (24, 25) was employed to determine whether repressive viral chromatin modifications that require Pol V, namely, augmented DNA methylation and deposition of H3K9me2, have a direct impact on chromatin organization. We also asked whether changes to the physical state of geminivirus chromatin influence gene expression. We report that Pol V-mediated increases in DNA and H3K9 methylation strongly correlate with a dramatically increased proportion of compacted viral chromatin and decreased viral gene expression during host recovery. Thus, the Pol IV-RdDM pathway required for recovery is linked to physical alteration of viral chromatin that negatively impacts viral gene expression. We additionally examined the expression levels of selected endogenous TEs, as geminivirus silencing suppressors are capable of inhibiting cellular DNA methylation and activating TE expression. Surprisingly, we found that in the absence of the viral suppressor that inhibits methylation and activates expression of transposable elements, the recovery state triggers a Pol V-dependent hypersuppression of two retrotransposons, such that very-low-level expression from these normally silenced elements is even further decreased. However, in these cases, hypersuppression does not strongly correlate with increased DNA and H3K9 methylation, suggesting a novel and as yet uncharacterized role for Pol V in chromatin organization.

RESULTS

The FAIRE assay discriminates between open and compact chromatin in mature *Arabidopsis* tissue. Previous experiments using FAIRE with *Arabidopsis* tissue extracts have distinguished nucleosome-depleted regions in the context of immature seedlings (26). Our experimental system involves geminivirus inoculation of plants in a long day growth cycle and culminates in symptomatic inflorescences. Thus, we confirmed the accuracy of FAIRE in mature tissue by examining regions with known chromatin compaction states.

Beginning with silique and floral tissue extracts from uninfected wild-type *Arabidopsis* (Columbia ecotype; Col-0), FAIRE was used to compare chromatin structure at a housekeeping gene (glyceraldehyde-3-phosphate dehydrogenase; *GAPDH*) with a locus that is transcriptionally repressed (*Ta3*; a *Copia* family retrotransposon). DNA in FAIRE-soluble and -insoluble fractions was detected by quantitative PCR (qPCR) using primers to amplify a portion of the *GAPDH* promoter or the central region of a unique *Ta3* element. We found that only ~16% of the recovered *Ta3* DNA was present in the FAIRE-soluble fraction, consistent with the expectation that most chromatin at this repressed locus is relatively condensed (Fig. 1A). In contrast, more than 60% of the recovered *GAPDH* DNA was present in the FAIRE-soluble fraction, indicating that the majority of chromatin at this actively transcribed locus is relatively open (Fig. 1B).

Similar results were obtained with another *Arabidopsis* ecotype, Landsberg erecta (Ler-0), although the proportions of DNA present in the FAIRE-soluble fraction at both the *Ta3* and *GAPDH* loci were somewhat less than those observed in Col-0 (~6% and ~50%, respectively [Fig. 1C and D]). As *Arabidopsis* ecotypes are known to vary with respect to density of epigenetic marks such as DNA methylation (27), differences in chromatin compaction between ecotypes are not entirely unexpected. In any case, from this assessment of two differentially expressed loci in two *Arabidopsis* ecotypes, we concluded that FAIRE could be used to examine chromatin compaction in the desired tissues.

FAIRE analysis confirms increased viral chromatin compaction during host recovery. Geminivirus silencing suppressors, including BCTV L2, are able to inhibit repressive methylation and suppress TGS (6–9, 28). As a consequence, wild-type BCTV is able to generate robust and sustained infections in susceptible hosts, including *Arabidopsis* and *Nicotiana benthamiana*. However, when inoculated with BCTV lacking the silencing suppressor (BCTV *L2⁻*), wild-type plants exhibit a recovery phenotype characterized by symptom remission and greatly reduced viral DNA levels (5, 29). In our
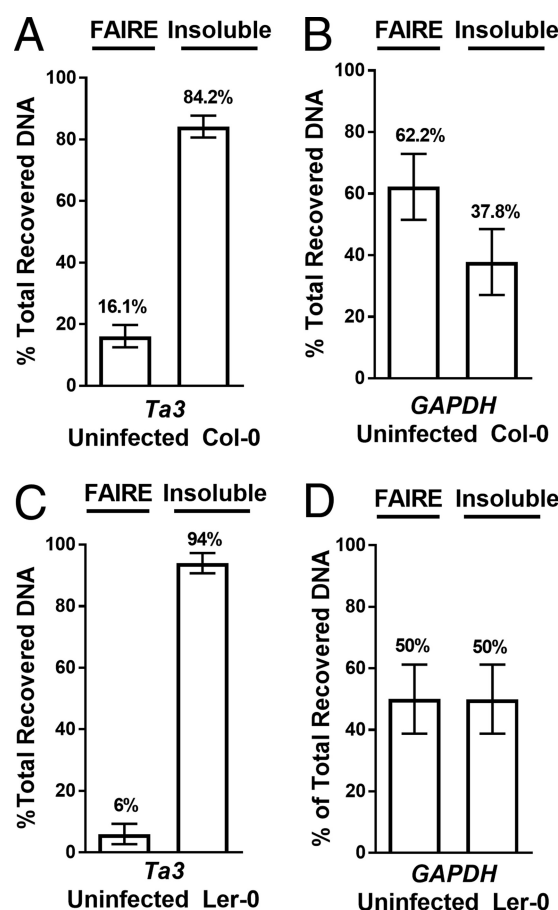
FIG 1 FAIRE distinguishes open and compact chromatin in mature *Arabidopsis* tissue. Extracts from silique and floral tissues of uninfected plants were analyzed to determine the relative amounts of FAIRE-soluble DNA indicative of relatively open chromatin and FAIRE-insoluble DNA characteristic of more highly condensed chromatin. The *Ta3* and *GAPDH* loci were assessed in wild-type *Arabidopsis* ecotype Col-0 (A and B) and ecotype Ler-0 (C and D). Histograms depict the average proportion of FAIRE-soluble versus -insoluble DNA as a percentage of total recovered DNA. Data were compiled from at least three biological replicates with at least two technical replicates each. Bars indicate standard errors.

system, initial BCTV *L2*⁻-infected shoots exhibit disease symptoms that include stunting and deformation of siliques and flowers. This primary tissue is harvested ∼21 days after inoculation. Shoots that later arise from axillary buds (secondary recovered tissue) contain low levels of viral DNA and lack symptoms. Most viral genomes in recovered tissue are hypermethylated in the intergenic region (IR), which contains divergent early and late gene promoters flanking the origin of replication. Further, Pol IV-RdDM is required, as *Arabidopsis* plants lacking components of this pathway (e.g., Pol V) fail to recover from BCTV *L2*⁻ and are unable to hypermethylate the IR (5, 16, 22).

Using the FAIRE assay, we asked whether differences in viral chromatin compaction levels could be observed between primary and recovered secondary tissues of wild-type *Arabidopsis* (Col-0) plants infected with BCTV *L2*⁻. Extracts were prepared and viral DNA was detected in FAIRE-soluble and -insoluble fractions using qPCR with primers to amplify the IR. Consistent with the presence of both active and repressed viral genomes in infected plants, in primary infected tissue, ∼43% of the viral DNA was in the FAIRE-soluble fraction indicative of open chromatin while ∼57% was in the insoluble fraction suggestive of compact chromatin (Fig. 2A). However, proportions were vastly different in recovered secondary tissue. Here less than 10% of BCTV *L2*⁻ IR DNA was detected in the FAIRE-soluble fraction, indicating that the majority of viral chromatin (>90%) is condensed during recovery (Fig. 2A). Greater compaction correlates with
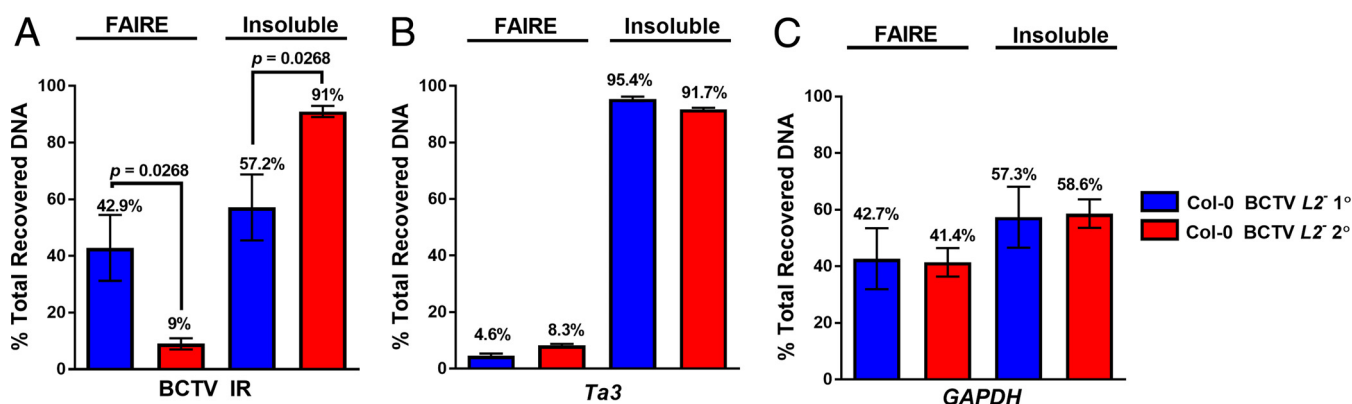
FIG 2 Host recovery correlates with an increase in compact viral chromatin. *Arabidopsis* (Col-0) plants were inoculated with BCTV *L2⁻*, and extracts obtained from primary and recovered secondary tissue were subjected to FAIRE analysis. (A) FAIRE using BCTV IR probes in symptomatic primary tissue (1°, blue bars) and asymptomatic recovered secondary tissue (2°, red bars). Control host loci *Ta3* (B) and *GAPDH* (C) were also examined in the same extracts. Data were compiled from at least three biological replicates, with at least two technical replicates each. Significance values were determined using Student's two-tailed *t* test. Bars indicate standard errors. (Note that *Ta3* and *GAPDH* data also appear in Fig. 4.).

previously observed increases in viral DNA methylation in recovered tissue and strongly suggests that this has a physical impact on viral minichromosomes, with the result being that most are converted to a more compact state.

Using the same extracts, analysis of *Ta3* and *GAPDH* revealed that both experienced a considerable reduction in the amount of FAIRE-soluble DNA in comparison to uninfected Col-0 plants (compare Fig. 2B and C with Fig. 1A and B). However, unlike viral minichromosomes, increased compaction at these endogenous loci was evident in both primary and secondary infected tissue. This enhanced compaction is consistent with host chromosome condensation previously observed in geminivirus-infected plants, where infected cells persist in a prophase-like state (30, 31). In the case of *Ta3*, the FAIRE-soluble, open chromatin fraction was reduced from ~16% in uninfected Col-0 plants to ~5% in primary infected tissue and remained low in recovered secondary tissue. At *GAPDH*, the proportion of open chromatin decreased from ~62% in uninfected Col-0 plants to ~43% in primary infected tissue and was not further decreased in recovered secondary tissue. Compaction at these loci is investigated further below (see Fig. 4).

Viral chromatin compaction requires Pol V. That RdDM is required for recovery suggests that this pathway is needed for viral chromatin compaction. Thus, the FAIRE assay was used with *Arabidopsis* mutants to examine the impact of Pol V deficiency on the state of viral chromatin. Pol V was selected because it is a key player in RdDM and is known to be required for host recovery, viral DNA hypermethylation, and H3K9me2 deposition on viral chromatin (16).

Before proceeding, it was necessary to determine if the absence of Pol V affects the proportion of viral ssDNA versus dsDNA in infected plants, as ssDNA is not bound by nucleosomes and presumably would partition in the FAIRE-soluble fraction. To do this, extracts were obtained from pools of at least three BCTV-infected plants to minimize plant-to-plant variation, and four independent pools each from wild-type and *pol V* mutant plants were treated with ScaI to linearize covalently closed and open circular BCTV dsDNA forms. Samples were then subjected to DNA blot analysis using ³²P-labeled BCTV oligonucleotide probes, and signals were quantitated as described in Materials and Methods. We observed that wild-type and *pol V* plants contained viral ssDNA and dsDNA in similar proportions (Fig. 3A) and concluded that ssDNA levels were unlikely to have a significant impact on FAIRE analysis.

Chromatin compaction levels were first compared between wild-type (Col-0) and *pol V* mutant plants inoculated with wild-type BCTV. Interestingly, despite the known antiviral functions of Pol V, little or no difference in the state of viral chromatin was noted, as between 30% to 35% of viral DNA was in the FAIRE-soluble fraction in both
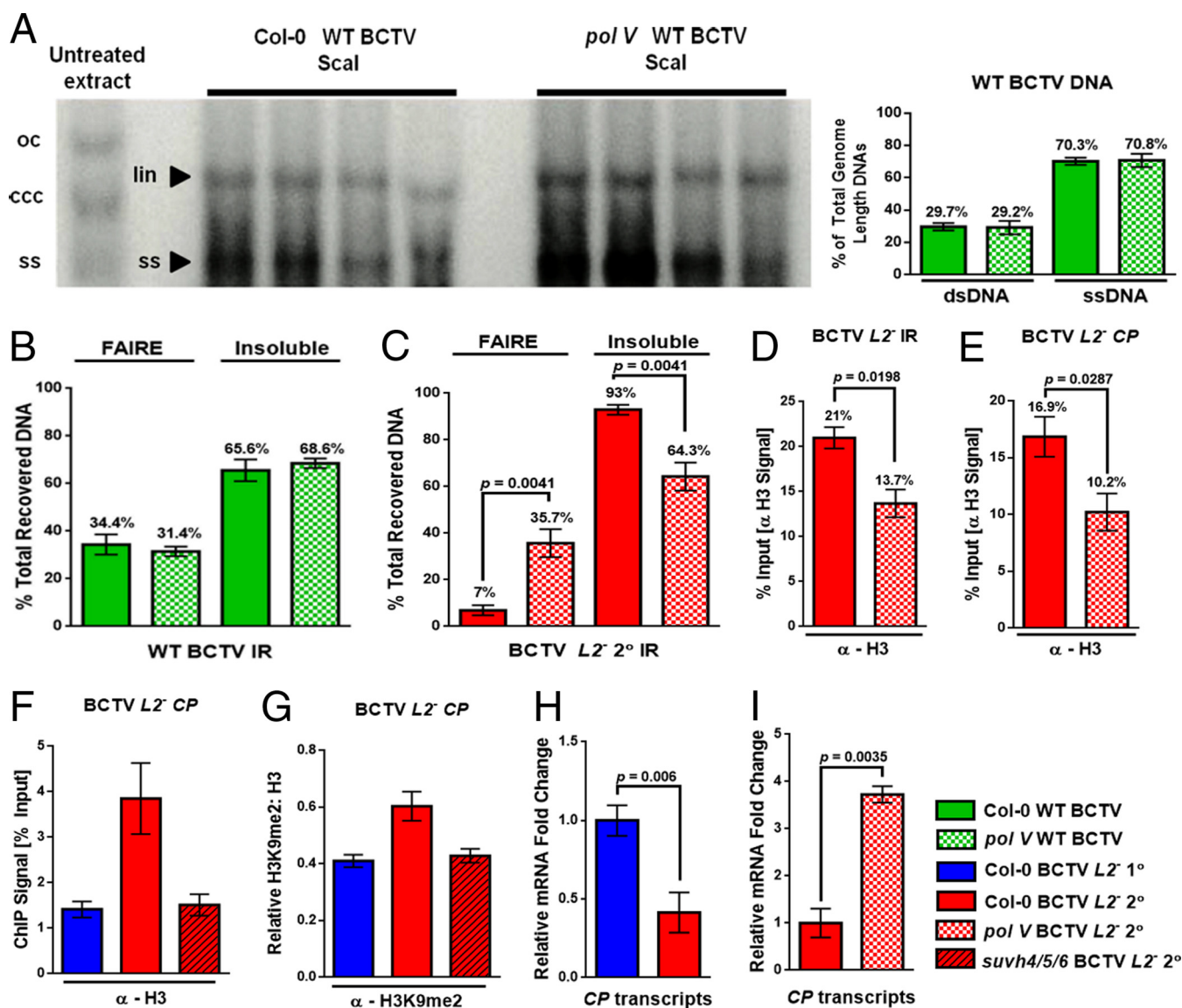
FIG 3 Pol V-dependent viral chromatin compaction correlates with increased nucleosome occupancy and H3K9 methylation and with reduced gene expression. (A) DNA blot analysis of BCTV DNA forms (left panel) in wild-type (WT) (Col-0) and pol V plants. Extracts were treated with ScaI to generate linear dsDNA from open circular (oc) and covalently closed circular (ccc) forms. Gel blots were hybridized with ^{32}P-labeled BCTV oligonucleotide probes. Percentages of total genome length linear dsDNA (lin) and ssDNA (ss), with standard error (SE), were compared (right panel). (B) FAIRE analysis using an IR probe with tissue from BCTV-infected wild-type and pol V plants. (C) Same as that described for panel B, except with secondary tissue from BCTV L2−-infected plants. (D and E) MNase-ChIP assays with secondary tissue from BCTV L2−-infected wild-type and pol V plants assessed H3 association (nucleosome occupancy) at the IR and CP CDS, respectively. Viral DNA immunoprecipitated with anti-H3 after MNase digestion was quantified as the percentage of total input. (F) ChIP using anti-H3 confirms increased nucleosome occupancy at the CP CDS during recovery. Extracts from BCTV L2−-infected primary and secondary tissue from wild-type plants were compared with secondary tissue from control suvh4/5/6 plants. Viral DNA precipitated with anti-H3 was quantified as a percentage of total input. (G) ChIP reveals increased H3K9me2 levels at the CP CDS during recovery. Extracts from BCTV L2−-infected primary and secondary tissue from wild-type plants were compared with secondary tissue from control suvh4/5/6 plants. Viral DNA precipitated with anti-H3K9me2 was quantified relative to H3 levels in comparable tissues. (H) CP expression is reduced in recovered tissue. Transcript levels in BCTV L2−-infected primary and secondary tissue were determined by RT-qPCR and normalized to a reference gene (PP2A) and to relative amounts of viral DNA, determined by qPCR. (I) Reduced CP expression is Pol V dependent. Transcript levels in BCTV L2−-infected secondary tissue from wild-type and pol V plants were measured as described for panel H. Data in panels B through I were compiled from at least three biological replicates, with at least two technical replicates each. Significance was evaluated using Student's two-tailed t test. Bars indicate standard errors.

wild-type and pol V plants (Fig. 3B). This is most likely due to the ability of the L2 suppressor to counter the effects of Pol V activity. However, results were quite different in asymptomatic, recovered secondary tissue of wild-type plants infected with BCTV L2−. Similar to previous experiments (Fig. 2A), in recovered secondary tissue, less than 10% of viral chromatin was in the FAIRE-soluble fraction, confirming that the vast

majority (>90%) is in a compact state during recovery. In contrast, significantly less compaction was evident in symptomatic, nonrecovered *pol V* secondary tissue where, like plants infected with wild-type virus, ~36% of viral DNA was in the FAIRE-soluble fraction (Fig. 3C). These results confirm that repressive viral chromatin modifications mediated by Pol V (and by extension RdDM) are essential for enhanced chromatin compaction and that the L2 suppressor protein efficiently counters these modifications.

Increased viral chromatin compaction is largely due to greater nucleosome occupancy. Both histone and nonhistone proteins (NHPs) can contribute to chromatin structure. This was illustrated by a recent study that revealed a small but significant impact of NHPs on the ability of micrococcal nuclease (MNase) to access chromatin-associated DNA (32). To determine the extent to which changes observed in viral chromatin compaction by the FAIRE assay are attributable to nucleosome occupancy, extracts from secondary tissue of wild-type and *pol V* plants infected with BCTV *L2⁻* were incubated with MNase, followed by chromatin immunoprecipitation (ChIP) with histone H3 antibody. MNase treatment was performed to obtain 1- to 3-nucleosome digestion efficiency (roughly equivalent to a maximum of ~650 bp of DNA), and viral DNA in immunoprecipitates was detected with the same IR-specific qPCR primers used for FAIRE. Primers to amplify a portion of the coat protein coding sequence (*CP* CDS) were also employed.

More viral chromatin was precipitated by H3 antibody in MNase-treated extracts from recovered wild-type plants than from nonrecovered *pol V* plants, indicating greater nucleosome association with viral IR DNA during recovery (Fig. 3D). Further, the disparity (21% versus 14%, a difference of ~33%) was similar to that observed using FAIRE (93% versus 64% insoluble DNA, a difference of ~31%) (Fig. 3C). A somewhat larger difference was evident with a *CP* CDS primer set, where an ~41% decrease in anti-H3-precipitated DNA was observed in *pol V* plants (~17% versus ~10%) (Fig. 3E). Thus, MNase-ChIP corroborates results obtained with FAIRE and in addition suggests that increased viral chromatin compaction during recovery is mostly due to greater nucleosome occupancy.

Enhanced viral chromatin compaction correlates with increased H3K9 methylation. In a previous study, we showed that Pol IV and Pol V occupy the BCTV *L2⁻* IR, but not the *CP* CDS, in primary tissue. However, both polymerases spread to *CP* CDS in recovered secondary tissue coincident with increased cytosine methylation (16). The same study also demonstrated that Pol IV and Pol V are required to amplify cytosine methylation at both the *CP* promoter-containing IR and the *CP* CDS and also to establish H3K9me2 on viral chromatin. To complement DNA methylation analysis, we compared H3K9me2 deposition levels at the BCTV *L2⁻ CP* CDS in primary and recovered secondary tissue. To do this in an unbiased manner, it was necessary to account for differences in nucleosome occupancy due to enhanced viral chromatin compaction during recovery.

ChIP using histone H3 antibody followed by qPCR with *CP* CDS primers confirmed FAIRE and MNase-ChIP results and showed that nucleosome occupancy is increased at this locus in secondary compared to primary tissue of wild-type plants infected with BCTV *L2⁻* (Fig. 3F). Interestingly, in control plants lacking SU(VAR)3-9 homologues SUVH4, -5, and -6, the three major H3K9 methyltransferases in *Arabidopsis* (33, 34), nucleosome occupancy in secondary tissue was similar to that observed in primary tissue from wild-type plants (Fig. 3F).

Next, ChIP experiments were carried out using H3K9me2 antibody. After normalization for H3 levels, we observed that the H3K9me2 signal at the *CP* CDS in primary tissue from wild-type plants was similar to that of control *suvh4/5/6* plants (Fig. 3G). Thus, consistent with the near absence of Pol IV and Pol V from the *CP* CDS during primary infection, there appears to be relatively little H3K9me2 at this locus in this stage. However, concordant with previously observed increases in cytosine methylation, H3K9me2 deposition was increased in recovered secondary tissue (Fig. 3G).

Enhanced viral chromatin compaction correlates with reduced gene expression. While changes in the proportion of FAIRE-soluble to -insoluble DNA often

correlate with altered gene expression, this is not always the case (25). To determine if increased BCTV *L2⁻* chromatin compaction observed during recovery impacts gene expression, we focused on the abundant *CP* transcript. Quantitative reverse transcriptase PCR (RT-qPCR) was performed to measure steady-state *CP* transcript levels in extracts obtained from BCTV *L2⁻*-infected primary and recovered secondary tissue. Transcript levels were normalized to the reference protein phosphatase 2a (*PP2A*) gene, which was unchanged in wild-type and *pol V* plants. Because recovered tissue contains much less viral DNA than nonrecovered tissue, transcript levels were then normalized to viral DNA levels determined by qPCR. Upon evaluating symptomatic primary tissue and nonsymptomatic secondary tissue from wild-type plants, an ~2.5-fold decrease in *CP* transcript levels was observed in the recovered tissue (Fig. 3H). We then compared recovered secondary tissue to secondary tissue from *pol V* plants and found that *CP* transcript levels were nearly 4-fold greater in the mutant plants (Fig. 3I).

Collectively, our results provide evidence that Pol V-dependent increases in nucleosome occupancy and physical compaction of viral chromatin that occur during recovery lead to decreased *CP* gene expression. Further, these outcomes correlate with increased cytosine and H3K9 methylation mediated by Pol V.

The recovery state impacts endogenous transposons. The BCTV L2 silencing suppressor inhibits methylation and as a result can increase transcription from silenced host loci, including TEs (6, 7, 9). However, because our recovery system relies on BCTV *L2⁻*, it provides a comparatively unfettered view of host defense capabilities, allowing us to ask whether the recovery state might also impact host chromatin. Thus, we examined whether Pol V contributes to compaction and silencing at endogenous genes and TEs during recovery.

Using FAIRE, uninfected *Arabidopsis* Col-0 plants exhibited fractionation of *Ta3* DNA similar to that observed earlier (compare Fig. 1A and 4A); however, the amount of insoluble DNA decreased from ~87% in wild-type plants to ~66% in uninfected *pol V* mutants (Fig. 4A). Nevertheless, the decline in *pol V* plants did not greatly compromise silencing, as it correlated with only a moderate increase in *Ta3* transcription (~1.5-fold) that did not achieve statistical significance (Fig. 4B). This suggests that while Pol V plays a role in chromatin compaction at *Ta3*, independent maintenance pathways appear sufficient to sustain TE silencing (see Discussion). As anticipated, chromatin status and transcription levels were essentially unaffected by the *pol V* mutation at *GAPDH*, which is not a Pol V target (Fig. 4C and D).

It should be noted here that *GAPDH* transcripts in wild-type plants were far more abundant than those from the repressed *Ta3* locus, as $2^{\Delta\Delta CT}$ values indicated ~60 versus 0.05 transcripts relative to the same *PP2A* reference gene, respectively. *Ta3* transcripts are essentially detectable only by RT-qPCR. Further, as RT was carried out using oligo(dT) primers, it is unlikely that noncoding Pol IV and Pol V RNAs, which are not polyadenylated, contributed to the *Ta3* transcript levels reported here (35–38) (our unpublished data).

As previously noted, both *Ta3* and *GAPDH* exhibited increased compaction in primary tissue infected with BCTV *L2⁻* compared to uninfected plants; compaction was not further increased in recovered secondary tissue (compare Fig. 1A and B with Fig. 2B and C). Again, at *Ta3*, the proportion of insoluble DNA in primary infected tissue (~95%) (Fig. 4E) was greater than in uninfected wild-type plants (~87%) (Fig. 4A). However, unlike uninfected plants, in primary tissue, chromatin compaction levels at *Ta3* were essentially unchanged by the absence of Pol V (Fig. 4E), and transcription was not significantly increased (Fig. 4F). Similarly, at *GAPDH*, the fraction of insoluble DNA in primary infected tissue (~57%) (Fig. 4G) was greater than in uninfected wild-type plants (~25%) (Fig. 4C), and compaction and transcription of *GAPDH* were not significantly altered by the *pol V* mutation (Fig. 4G and H). Thus, increased compaction at *Ta3* and *GAPDH* observed in primary infected tissue compared to uninfected tissue appears to be general and Pol V independent.
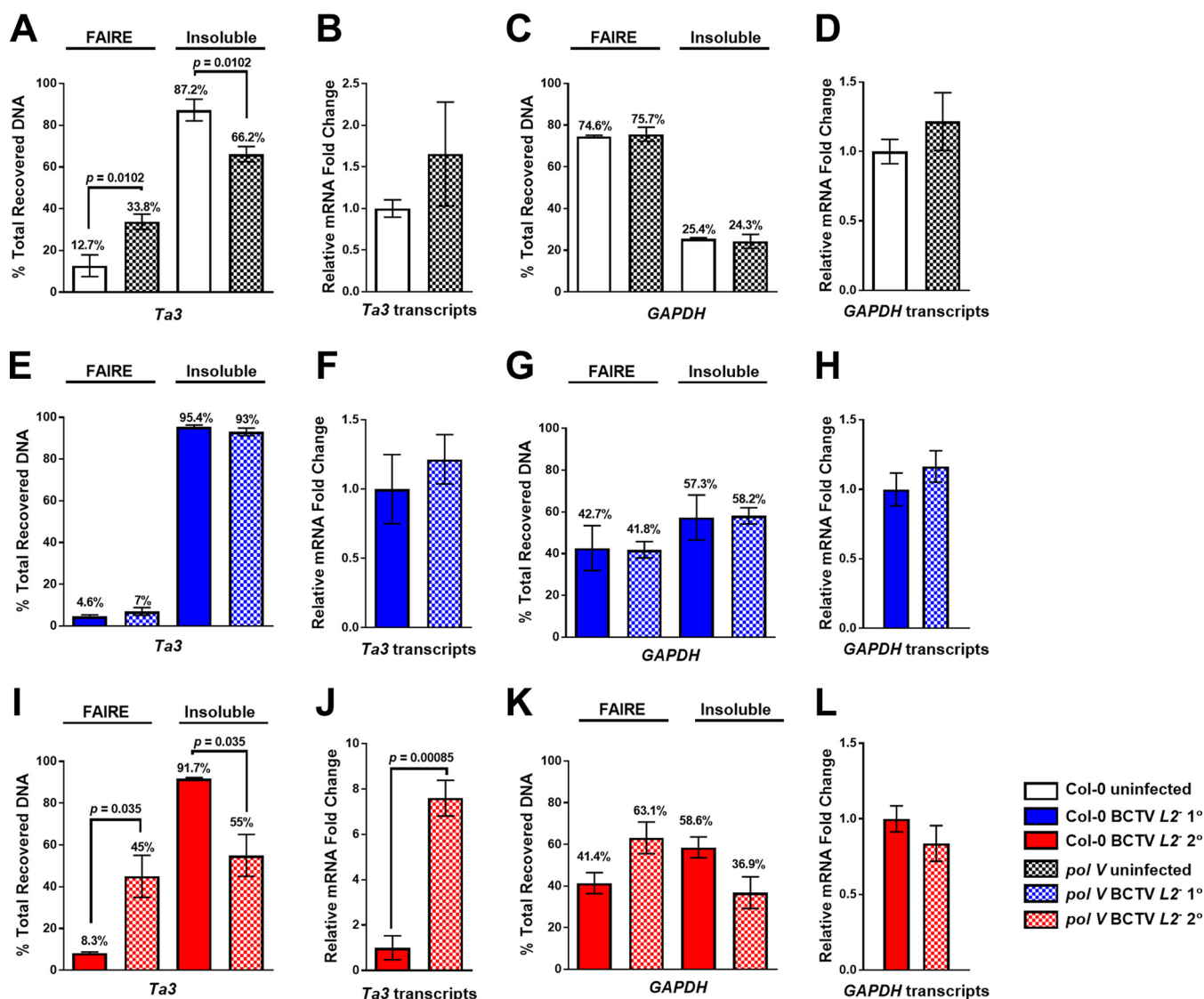
FIG 4 Pol V contributes to *Ta3* suppression during recovery. Comparative FAIRE and RT-qPCR analyses were carried out for the *Ta3* and *GAPDH* loci with tissue from wild-type and *pol V* plants. Transcript levels measured by RT-qPCR were compared to the *PP2A* reference gene. (A to D) Tissue from uninfected plants; (E to H) primary tissue from BCTV *L2⁻*-infected plants; (I to L) secondary tissue from BCTV *L2⁻*-infected plants. Data were compiled from at least three biological replicates, with at least two technical replicates each. Significance values were determined using Student's two-tailed *t* test. Bars indicate standard errors. (Note that FAIRE data for *Ta3* and *GAPDH* with wild-type plants in panels E and G, respectively, are also shown in Fig. 2B and C. Experiments with wild-type and *pol V* plants were carried out in parallel.)

Results were quite different in recovered secondary tissue from BCTV *L2⁻*-infected plants. Here, the fraction of insoluble compact chromatin was greatly reduced in *pol V* plants (from ~92% to ~55%) (Fig. 4I), and this correlated with a large increase (>7-fold) in *Ta3* transcript levels (Fig. 4J). This also contrasts with the situation in uninfected plants, where Pol V deficiency resulted in a more moderate reduction in compaction that did not greatly increase *Ta3* transcription (Fig. 4A and B). This suggests that during recovery, a Pol V-dependent mechanism acts to further reinforce *Ta3* silencing. Insoluble compact chromatin was also somewhat reduced at *GAPDH* in *pol V* plants (~59% to ~37%) (Fig. 4K), although this reduction was not statistically significant and did not correlate with increased transcription (Fig. 4L).

To extend this analysis, transcript levels of *ACTIN* and *Athila6A*, a Gypsy class retrotransposon, were compared in wild-type and *pol V* plants infected with BCTV *L2⁻*. *Athila6A* was selected as its regulation appears to differ from that of *Ta3* (39, 40). However, reminiscent of *Ta3*, a comparatively moderate increase in *Athila6A* transcript
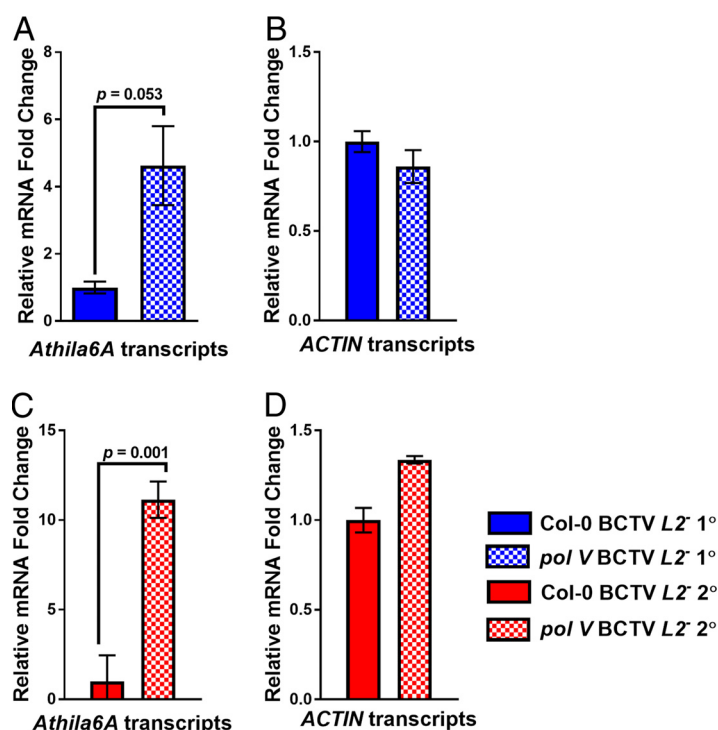
FIG 5 Pol V also contributes to *Athila6A* suppression during recovery. Comparative RT-qPCR analyses were carried out at the *Athila6A* and *ACTIN* loci with tissue from wild-type and *pol V* plants. Levels were compared to those of the *PP2A* reference gene. (A and B) Primary tissue from BCTV *L2⁻*-infected plants; (C and D) secondary tissue from BCTV *L2⁻*-infected plants. Data were compiled from at least three biological replicates, with at least two technical replicates each. Significance values were determined using Student's two-tailed *t* test. Bars indicate standard errors.

levels (~4-fold) was detected in *pol V* plants relative to wild-type plants in primary tissue (Fig. 5A), while a very large increase (>10-fold) was observed in secondary tissue (Fig. 5C). *ACTIN* transcript levels were similar between wild-type and *pol V* plants in both primary and secondary tissue (Fig. 5B and D).

In summary, these results suggest that during primary infection with BCTV *L2⁻*, a Pol V-independent, generalized compaction of host chromatin occurs that does not greatly impact transcript levels. In comparison, in secondary tissue, loss of Pol V resulted in large increases in TE transcription but did not affect expression of the housekeeping loci examined.

TE transcripts are reduced below levels in uninfected plants during host recovery. To better appreciate observed changes in transcript levels, we compared some of the data used to generate Fig. 4 and 5 in different ways. First, differences between primary and recovered secondary tissue infected with BCTV *L2⁻* were contrasted. Similar to the decrease in viral *CP* transcription observed during recovery (Fig. 3H), steady-state levels of *Ta3* and *Athila6A* transcripts were decreased between ~3.0- to 3.5-fold in recovered secondary tissue relative to primary tissue (Fig. 6A and B). These decreases in viral and TE transcription are Pol V dependent (Fig. 3I, 4J, and 5C). Further, as TE expression is normally repressed, the additional decrease can be viewed as hypersuppression. In contrast, *GAPDH* transcript levels increased ~2-fold in secondary compared to primary infected tissue (Fig. 6C), while *ACTIN* transcription was unchanged (Fig. 6D).

Next, transcript levels were compared between uninfected plants and BCTV *L2⁻*-infected, recovered secondary tissue. This confirmed hypersuppression of *Ta3* and *Athila6A*, as transcript levels were ~4- and ~2.5 lower, respectively, in recovered tissue than in uninfected plants (Fig. 6E and F). In contrast, *GAPDH* and *ACTIN* transcript levels were similar in both uninfected and secondary tissues (Fig. 6G and H).
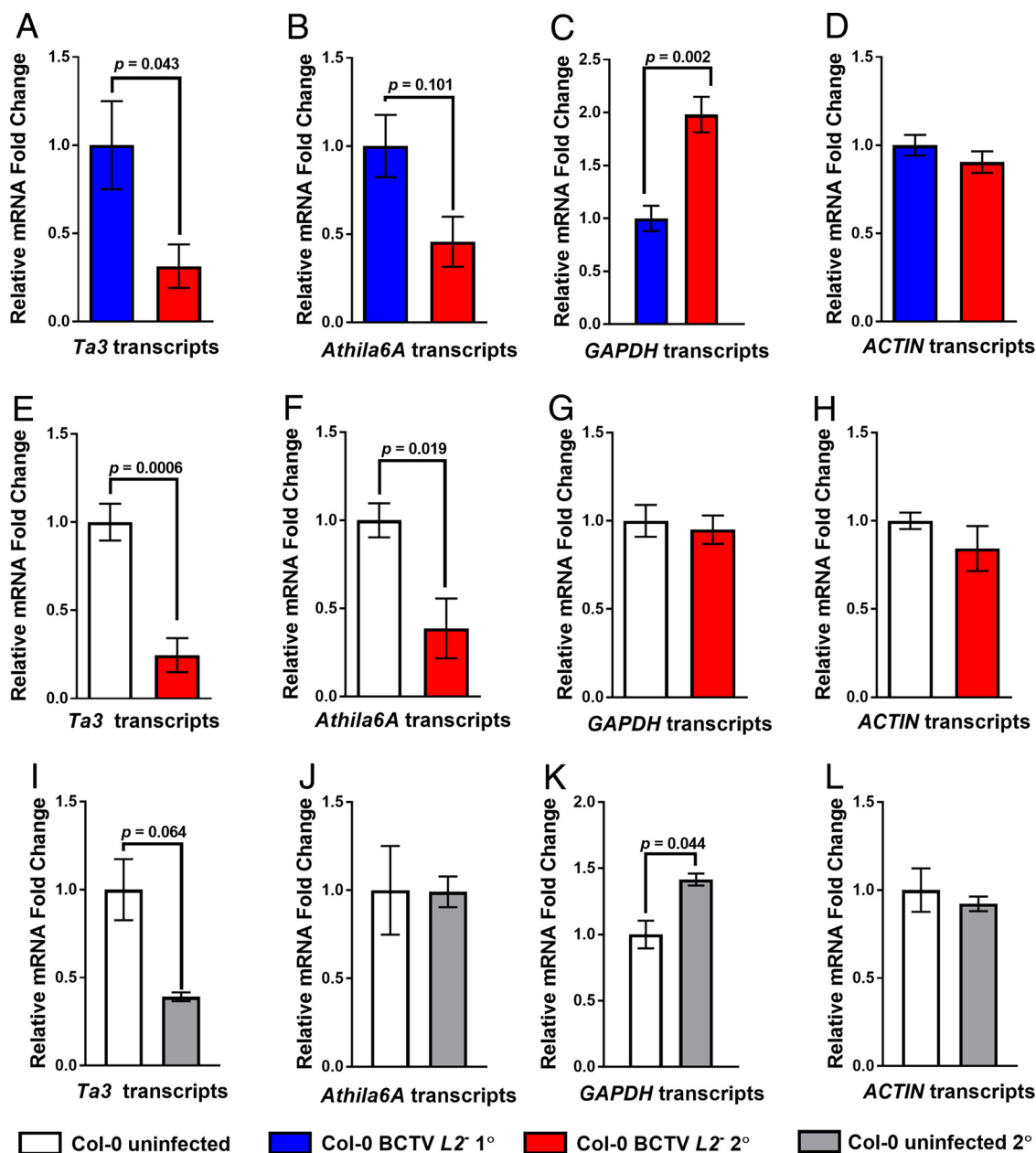
FIG 6 Suppression of *Ta3* and *Athila6A* is bolstered by the recovery state. Transcript levels determined for *Ta3*, *Athila6A*, *GAPDH*, and *ACTIN* are shown. (A to D) Comparisons between BCTV *L2*⁻-infected primary and recovered secondary tissues; (E to H) comparisons between uninfected tissue and BCTV *L2*⁻-infected recovered secondary tissues (note that data for these comparisons were taken from Fig. 5 and 6); (I to L) comparison between tissues from uninfected *Arabidopsis* plants harvested to mimic the recovery assay. Tissue was collected from healthy plants at the developmental stage when inoculation is performed and from secondary tissues arising from axillary buds 4 weeks later, after initial bolts (primary tissue) were removed. Data were compiled from at least three biological replicates, with at least two technical replicates each. Significance values were determined using Student's two-tailed *t* test. Bars indicate standard errors.

While the data suggest that the recovery state triggers hypersuppression of the transposable elements (TEs) *Ta3* and *Athila6A*, we considered the possibility that developmental changes in TE expression might also occur. Thus, expression levels were examined using tissues from uninfected *Arabidopsis* plants harvested to mimic the recovery assay. Tissue was collected from healthy plants at the developmental stage when inoculation is performed and from secondary tissues arising from axillary buds 4 weeks later, after initial bolts (primary tissue) were removed. We found that *Ta3* expression levels appeared to decline ~2.5-fold in uninfected secondary tissue (Fig. 6I),

although this did not achieve statistical significance and was less than the significant reduction observed in secondary recovered tissue from BCTV $L2^-$-infected plants (~4-fold) (Fig. 6E). *Athila 6A* transcript levels in uninfected plants were similar regardless of developmental stage (Fig. 6J), and thus the reduction observed during recovery in BCTV $L2^-$-infected plants (~2.5-fold) (Fig. 6F) could be fully attributed to host recovery. In contrast, *GAPDH* expression was increased (~1.5-fold) (Fig. 6K) in secondary tissue from uninfected plants, while *ACTIN* expression was unaffected (Fig. 6L). Together, these results indicate that the recovery state results in Pol V-dependent hypersuppression of *Ta3* and *Athila6A* transcription.

Reduced TE expression does not strictly correlate with increased DNA and H3K9 methylation. Recovery resulted in significantly reduced expression of the viral *CP* gene and hypersuppression of *Ta3* and *Athila6A*. As these events require Pol V, it was natural to assume that reduced transcription should correlate with increased DNA and H3K9 methylation. Increased cytosine methylation and H3K9me2 levels during recovery have already been documented at the *CP* promoter and the *CP* CDS (Fig. 3G) (16). Thus, bisulfite sequencing was carried out to assess cytosine methylation at *Ta3* and *Athila6A* in uninfected plants and recovered secondary tissue from BCTV $L2^-$-infected plants. The central region of *Ta3* analyzed contains 85 cytosines in the following contexts: 1 CG, 30 CHG, and 54 CHH (where H is any nucleotide except G). The region of the *Athila6A* long terminal repeat (LTR) analyzed contains 75 cytosines, including 15 CG, 15 CHG, and 45 CHH.

We observed that cytosine methylation levels in all sequence contexts were generally similar at both of the TEs in uninfected plants (Fig. 7A and B). Total cytosine methylation was reduced ~10% in recovered compared to uninfected tissue at *Ta3*, but no difference was evident at *Athila6A*. Further, CHH methylation was relatively low at both TEs, consistent with methylation patterns being largely sustained by maintenance pathways independent of RdDM (13, 41). In comparison, CHH methylation constitutes a much larger fraction of the total at the BCTV IR and *CP* CDS, a feature characteristic of active RdDM (16, 22).

ChIP with anti-H3K9me2, normalized to H3 levels, was carried out to compare H3K9 methylation at *Ta3* and *Athila6A* between uninfected and infected but recovered tissues. As expected, in uninfected plants, substantial H3K9me2 signal was evident at both TEs relative to *suvh4/5/6* control plants. Similar to the BCTV *CP* CDS (Fig. 3G), H3K9me2 signal was increased at *Ta3* in recovered secondary tissue, although this was not observed at *Athila6A* (Fig. 7C and D). Thus, despite Pol V dependence and in contrast to viral chromatin, the hypersuppression of *Ta3* and *Athila6A* observed during recovery does not correlate with increased cytosine methylation and is coincident with increased H3K9 methylation only in the case of *Ta3*.

DISCUSSION

Previous studies from our laboratory demonstrated that host recovery from BCTV $L2^-$, which lacks a suppressor that inhibits methylation (6, 9), is accompanied by hypermethylation of the viral IR. Mutant plants deficient for Pol IV-RdDM pathway components are unable to recover and fail to hypermethylate the IR. In addition, we showed that viral chromatin is associated with epigenetic marks characteristic of gene repression (high levels of DNA methylation and H3K9me2) or active gene expression (low levels of DNA methylation and H3K9/14ac). The equilibrium between them dictates the outcome of infection; an abundance of repressed chromatin favors host recovery (5, 16, 22). A recent study supported this concept by showing that two populations of viral minichromosomes are present in pepper plants infected with PepGMV, which provides an example of a natural recovery system. In symptomatic tissue, the majority of minichromosomes (50 to 70%) were found to be in a relatively open state, while most (55 to 75%) were highly condensed in asymptomatic, recovered tissue. Compacted minichromosomes were associated with high levels of DNA and H3K9 methylation suggestive of transcriptional silencing, while most open minichromosomes exhibited DNA hypomethylation and an active mark (H3K4me3) (23).
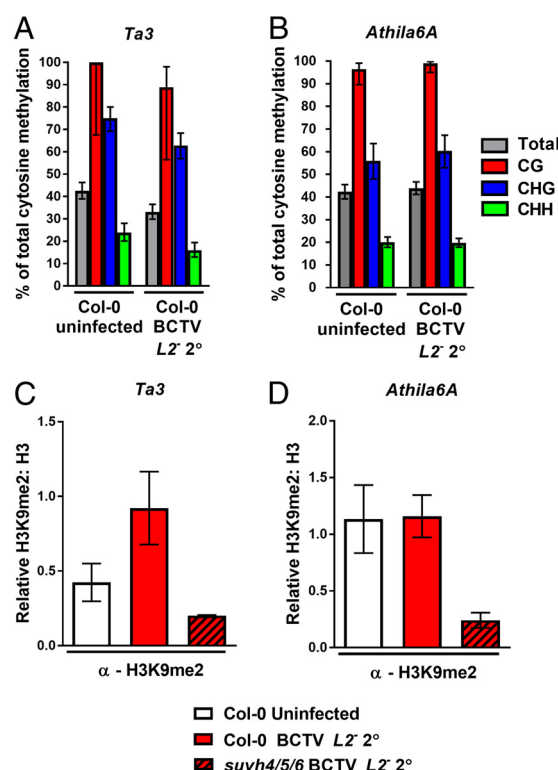
FIG 7 Reduced TE expression does not strictly correlate with increased cytosine and H3K9me2 levels. Methylation status of *Ta3* (A) and *Athila6A* (B) in uninfected plants and in recovered secondary tissue from BCTV *L2⁻*-infected plants. Samples consisted of tissue pooled from at least three plants. DNA was treated with bisulfite, and PCR was performed using primers to amplify the central region of *Ta3* or a portion of the *Athila6A* LTR. PCR products were cloned and sequenced (6 to 9 per treatment). Histograms show the percentage of methylated cytosines in different sequence contexts: CG in red, CHG in blue, and CHH in green. Total methylation is indicated in gray. Bars indicate Wilson score interval 95% confidence limits. ChIP experiments were performed to determine H3K9me2 levels at *Ta3* (C) and *Athila6A* (D) in uninfected plants and in recovered secondary tissue from BCTV *L2⁻*-infected plants. DNA precipitated with anti-H3K9me2 was detected by qPCR using primers to amplify portions of the *Ta3* and *Athila6A* LTRs, and data were normalized relative to H3 levels in comparable tissues. H3K9me2 levels relative to H3 levels in wild-type and control *suvh4/5/6* plants were then compared. Data were compiled from at least three biological replicates with at least two technical replicates each. Bars indicate standard errors.

The studies described in this communication confirm and extend our knowledge of how the recovery state impacts viral chromatin structure and activity and of the role of Pol IV-RdDM in recovery. In short, our results unambiguously link the Pol IV-RdDM pathway involving Pol V to enhanced viral chromatin compaction and reduced viral gene expression. We used FAIRE to verify that both open and compacted viral chromatin exists in infected *Arabidopsis* plants and found that the vast majority is condensed in recovered secondary tissue from BCTV *L2⁻*-infected plants. The absence of the silencing suppressor may explain why a greater proportion of compacted chromatin was observed in our studies (91% to 93%) than with PepGMV (55% to 75%). Using an MNase-ChIP assay, we further showed that enhanced compaction was mostly due to increased nucleosome occupancy. Bisulfite sequencing and ChIP experiments confirmed the correlation between enhanced compaction and increased cytosine and H3K9 methylation. Finally, we established that these phenomena culminate in a significant reduction in viral *CP* transcript levels.

By including *pol V* mutant plants in our studies, we additionally demonstrated that enhanced viral chromatin compaction and suppressed viral gene expression require Pol V activity and by extension the Pol IV-RdDM pathway. Combined with the studies discussed above, this body of work conclusively demonstrates that repressive methylation of geminivirus chromatin, conditioned by RdDM, is a major host defense against geminiviruses that leads to physical compaction of viral chromatin and reduced viral

gene expression. Hence, mutations that compromise RdDM result in hypersusceptibility and the absence of host recovery. The observation that *Ty-1*, an economically important tomato resistance gene, encodes an RDR that conditions enhanced methylation of *Tomato yellow leaf curl virus* DNA offers another and perhaps more practical illustration of the importance of methylation-mediated defense against geminiviruses (42).

As a cautionary note, both FAIRE and ChIP are based on fractionation of chromatin fragments sheared to between 200 and 800 bp in size, and thus it is possible that the increased nucleosome density observed at the IR during recovery might not extend to the entire minichromosome. This argument also applies to analysis of control genes and TEs. However, we note that MNase ChIP data suggest similar nucleosome densities at the IR and CP regions (Fig. 3C and D).

Taking advantage of the ability of BCTV *L2⁻* to systemically infect plants, we also examined the effects of host recovery on endogenous loci. Our rationale that the absence of the suppressor protein permits a clearer view of host defenses is bolstered by experiments that compared viral chromatin compaction levels in wild-type and *pol V* plants infected with wild-type BCTV or BCTV *L2⁻* (Fig. 3B and C). These showed that while the proportions of open BCTV chromatin were similar in wild-type and *pol V* plants (∼30% to 35%), the extremely low levels of open BCTV *L2⁻* chromatin in recovered wild-type plants (<10%) were restored to ∼36% in *pol V* plants. Thus, L2 protein effectively opposes the antiviral activities of Pol V.

While Pol IV-RdDM plays an important role in host genome homeostasis by rein-forcing transcriptional silencing of heterochromatic loci such as TEs, once established, DNA and H3K9 methylation can also be propagated by mechanisms that do not involve small RNAs (12–14). In this case, repressive methylation is maintained by feed-forward loops involving H3K9 methyltransferases, such as SUVH4 that bind methylated DNA, and cytosine methyltransferases, including methyltransferase 1 (MET1) and the H3K9-binding chromomethylase 2 (CMT2) and CMT3 (43). Thus, we also asked whether the absence of Pol V affects cellular chromatin compaction and transcription during BCTV *L2⁻* infection. Loci examined included the retrotransposons *Ta3* and *Athila6A*, which are essentially silenced in wild-type plants, and euchromatic housekeeping genes *GAPDH* and *ACTIN*.

In uninfected plants, loss of Pol V led to a decrease in chromatin compaction at *Ta3* coincident with a modest increase in transcript levels, suggesting that while Pol IV-RdDM plays a role in reinforcing methylation-mediated TGS, the aforementioned maintenance pathways are sufficient to sustain it at this locus. On the other hand, the absence of Pol V had no apparent effect on the *GAPDH* locus, which is not a target of RdDM (Fig. 4A to D). Further investigation revealed two distinct impacts of viral infection on host chromatin. First, during primary infection with BCTV *L2⁻*, a Pol V-independent compaction of both *Ta3*- and *GAPDH*-associated chromatin was observed. However, loss of Pol V did not significantly alter expression of *Ta3*, *GAPDH*, and *ACTIN*, although *Athila6A* transcript levels experienced an increase of ∼4-fold (Fig. 4E to H and 5A and B). Why this might be is not clear, but geminivirus infection has complex effects on host gene expression, with transcript levels of some genes being increased while others are decreased (44). In any case, generalized compaction during primary infection likely reflects the condensation and marginalization of host chromatin previously observed in geminivirus-infected cells (30, 31). Compaction and relocation of host chromatin to the nuclear periphery as virus replication centers expand to occupy much of the organelle is a common feature of DNA virus infections (45, 46).

The second impact of BCTV *L2⁻* infection was observed in recovered secondary tissue. Here the absence of Pol V resulted in a large decrease in compaction at *Ta3*, accompanied by substantial increases in *Ta3* and *Athila6A* transcript levels (>7-fold and >10-fold, respectively), suggesting that Pol V acts to robustly reinforce TE silencing during recovery. This is a targeted effect, as levels of *GAPDH* and *ACTIN* transcripts were essentially unaltered (Fig. 4I to L and 5B and D). Therefore, despite the fact that compaction levels as measured by FAIRE were similar in primary and secondary tissue, the functional state of TE chromatin differs, as compaction becomes Pol V dependent

in secondary tissue, and substantial increases in TE expression were observed in the absence of this enzyme. This functional difference was underscored by a direct comparison of TE transcript levels in primary and recovered secondary tissue (Fig. 6A and B) and between uninfected and recovered tissue (Fig. 6E and F). This revealed a hypersuppression of both *Ta3* and *Athila6A* during recovery similar to that observed for the viral *CP* gene, such that expression was reduced below levels seen in uninfected plants. Surprisingly, however, Pol V-dependent hypersuppression of *Ta3* and *Athila6A* did not correlate with enhanced DNA methylation (Fig. 7A and B), and H3K9 methylation appeared to increase only at *Ta3* (Fig. 7C and D).

Analogous to "systemic acquired silencing" (47), the trigger for host recovery is likely a mobile signal that specifically identifies the virus and primes host defenses in newly emerging tissues and tissues distant from the site of primary infection (48–50). The requirement of Pol IV-RdDM for recovery indicates that the signal likely consists of systemically mobile 24-nt siRNAs (51–53). Virus-derived small RNAs that reach tissues in advance of the virus could act as "homology sensors," enabling Pol IV-RdDM to efficiently recognize and apply repressive methylation to viral chromatin that is formed *de novo* in infected cells. This process resembles the homology-dependent silencing observed when TEs become activated or are transgenically introduced into a genome containing silenced copies of a cognate TE (13, 41, 54–56), and our data suggest that a similar mechanism underpins host recovery from geminivirus infection.

However, as TE-derived 24-nt siRNAs are normally abundant and ubiquitous, TE hypersuppression argues that recovery may involve an additional Pol V-dependent response that enhances silencing but may not strictly correspond with classical outputs of Pol IV-RdDM. Several observations support this view. First, hypersuppression did not correlate with increased cytosine methylation at *Ta3* and *Athila6A*, and the low levels of CHH methylation seen at these loci were instead indicative of maintenance by cytosine methyltransferase CMT2 (Fig. 7A and B). Further, while H3K9 methylation levels were somewhat elevated at *Ta3* during recovery, they were not increased at *Athila6A* (Fig. 7C and D). In light of these negative correlations, we suggest that bolstered TE suppression is due, at least in part, to a currently uncharacterized mechanism. Further, because TE chromatin compaction levels were similar in primary and recovered secondary tissue, we speculate that functional differences might be the result of differential nucleosome positioning and/or recruitment of nonhistone proteins. While these possibilities were not investigated here, we note parallels with other studies that have implicated SUVR2, a SUVH4-related protein that lacks histone methyltransferase activity, in transcriptional silencing at Pol IV-RdDM target loci. SUVR2 has been identified as a Pol IV-RdDM pathway component, but although its loss impaired TGS at tested TEs and transgenes, *suvr2* mutants exhibit weak reductions in cytosine methylation (57, 58). Interestingly, SUVR2 interacts with multiple putative chromatin remodelers related to SNF2 (58, 59). Whether TE hypersuppression during recovery involves SUVR2 and these chromatin remodelers remains to be determined.

Why does the recovery state impact both viral and TE-associated chromatin? Mechanistically, as noted above, a common suppression pathway provides a likely explanation. Biologically, an obvious benefit of recovery is that the low levels of virus and absence of disease symptoms permit relatively normal development of floral tissues, increasing host reproductive capacity. A defense that targets DNA viruses as well as TEs, which can be activated by stress (55), would be advantageous in these circumstances. Such a response could simultaneously inhibit virus replication and enforce tighter control over TEs to maintain genome integrity in infected tissues destined to give rise to the next generation. A novel observation from our work is that TE suppression during recovery is even greater than that seen in uninfected, wild-type plants. This hypersuppression is likely to be especially important for natural recovery from wild-type geminiviruses, as their L2 and AL2 suppressor proteins can inhibit methylation and cause ectopic expression of TEs (6, 9).

MATERIALS AND METHODS

Plant materials and inoculation. *Arabidopsis thaliana* Columbia (Col-0) or Landsberg erecta (Ler-0) plants were grown in SunGro professional growing mix at 22°C with an 18-h-light/6-h-dark cycle in a growth room. Studies with mutant plants employed the following transfer DNA (T-DNA) insertion lines, all in the Col-0 background: the *nrpdb-11* mutant, lacking the large catalytic subunit of Pol V (SALK_029919) (60), and the *suvh4/5/6* H3K9 methyltransferase triple mutant (SALK_046606, SALK_074957, and SAIL_865_E08, respectively) (33, 34). The homozygosity of all mutants was verified by genotyping.

Plants were agroinoculated with *Beet curly top virus* (BCTV) or mutant viruses lacking the L2 silencing suppressor (BCTV *L2-1* or BCTV *L2-2*, here referred to as BCTV *L2⁻*) (29), as previously described (5). Tissue was harvested 21 to 25 days postinoculation (primary infected tissue). Shoots arising later from axillary buds (secondary tissue) were collected 5 weeks postinoculation. Tissues collected included floral heads and siliques.

FAIRE assay. The FAIRE assay utilized by Arbuckle and Kristie (25) was adapted for use with mature *Arabidopsis* plants, with the following modifications. Tissue (300 to 600 mg) collected from three to six plants was cross-linked with paraformaldehyde, and nuclei were isolated from ground tissue according to the method of Shu et al. (61). Following isolation, nuclei were resuspended and lysed in solution with a plastic loop (26). Chromatin was sheared by sonication to produce fragments ranging in size from 200 to 800 bp, and 10% of the DNA was set aside as an input fraction. Recovery of FAIRE-soluble and -insoluble DNA was as described previously (25).

Quantitative PCR (qPCR) was used to measure DNA in the FAIRE-soluble and -insoluble fractions with primers to amplify the BCTV intergenic region (IR) and cellular loci (*Ta3* and *GAPDH*). qPCR was performed as described previously (16). Primer sequences are available upon request.

DNA blot analysis and measurement. Extracts were obtained from pooled tissues of at least three infected plants to minimize plant-to-plant variation. Approximately 600 ng of extracted DNA was digested overnight at 37°C with ScaI, which cleaves at a single site within the viral genome. Samples were subjected to DNA blot analysis with ³²P-labeled, BCTV-specific oligonucleotide probes prepared using T4 polynucleotide kinase (Thermo Fisher Scientific). Blot membranes were exposed to a phosphoimager screen overnight, and signals were detected using a Bio-Rad PMI system. Levels of ssDNA and dsDNA were measured as pixel density with Bio-Rad Quantity One Imager software.

MNase and ChIP assays. Nuclei were isolated from secondary tissue from BCTV *L2⁻*-infected wild-type and *pol V* plants as described previously (62). Nuclear pellets were flash frozen in liquid nitrogen and resuspended on ice in MNase reaction buffer (10 mM Tris [pH 8.0], 15 mM NaCl, 60 mM KCl, 0.15 mM spermine, 0.5 mM spermidine, 10 mM CaCl₂) with a plastic loop. One gel unit (200 Kunitz units) of micrococcal nuclease (MNase; New England BioLabs) and 20 μg RNase A (Thermo Fisher Scientific) were added to the resuspended nuclei and left at 37°C for 30 min with occasional mixing. Samples were then placed on ice, and EDTA and EGTA were added to a final concentration of 10 mM each to stop the reaction. Samples were sonicated twice briefly (10 s, low setting) using a Diagenode Bioruptor. Chromatin immunoprecipitation (ChIP) lysis buffer was then added to a final concentration of 50 mM HEPES (pH 7.5), 150 mM NaCl, 1% Triton X-100, 0.1% Na deoxycholate, 0.1% SDS, 10 mM Na butyrate, 50 mM Na orthovanadate, 30 mM NaF, 1 mM phenylmethylsulfonyl fluoride (PMSF), and 1× protease inhibitor cocktail (Sigma), and the mixture was allowed to nutate at 4°C for 10 to 20 min. Samples were precleared with protein G resin (Genscript) for 3 h. Recovered supernatants were decanted into fresh tubes and incubated with anti-histone H3 (Genscript A-01502-40). The remaining steps were performed as previously reported (5), except that the final cleanup was done using DNA Clean and Concentrator-25 (Zymo). Viral DNA immunoprecipitated by anti-H3 was measured using qPCR.

Standard ChIP was performed with anti-H3 and anti-H3K9me2 (Abcam, ab1220) antibodies as previously described (16), and immunoprecipitated viral DNA or DNA corresponding to host loci was quantitated by qPCR.

DNA isolation, RNA isolation, and RT-qPCR. Samples were divided to isolate both DNA and RNA from the same extract. DNA was extracted using the Nucleospin Plant II kit (Macherey-Nagel) according to the manufacturer's protocol. RNA isolation employed PureLink plant RNA reagent (Thermo Fisher Scientific). cDNA was generated with SuperScript III reverse transcriptase (Thermo Fisher Scientific), and oligo(dT) primers (New England BioLabs). Primer sequences used for qPCR will be provided upon request. RNA levels were normalized to the protein phosphatase 2a (*PP2A*) reference gene using the ΔΔC_T method (63). *CP* transcript levels were also normalized to adjust for the amount of viral DNA template present. Viral DNA levels were normalized to 18S ribosomal DNA.

Bisulfite sequencing. Bisulfite sequencing of endogenous TE loci was performed as described previously (5), with minor modifications (41). Data were analyzed using Kismeth (64).

REFERENCES

1. Gu H, Roizman B. 2007. Herpes simplex virus-infected cell protein 0 blocks the silencing of viral DNA by dissociating histone deacetylases from the CoREST-REST complex. Proc Natl Acad Sci U S A 104:17134–17139. https://doi.org/10.1073/pnas.0707266104.

2. Cliffe AR, Knipe DM. 2008. Herpes simplex virus ICP0 promotes both histone removal and acetylation on viral DNA during lytic infection. J Virol 82:12030–12038. https://doi.org/10.1128/JVI.01575-08.

3. Liang Y, Vogel JL, Narayanan A, Peng H, Kristie TM. 2009. Inhibition of histone demethylase LSD1 blocks α-herpesvirus lytic replication and reactivation from latency. Nat Med 15:1312–1317. https://doi.org/10.1038/nm.2051.

4. Lee JS, Raja P, Knipe DM. 2016. Herpesviral ICP0 protein promotes two waves of heterochromatin removal on an early viral promoter during lytic infection. mBio 7:e02007-15. https://doi.org/10.1128/mBio.02007-15.

5. Raja P, Sanville BC, Buchmann RC, Bisaro DM. 2008. Viral genome methylation as an epigenetic defense against geminiviruses. J Virol 82:8997–9007. https://doi.org/10.1128/JVI.00719-08.

6. Buchmann RC, Asad S, Wolf JN, Mohannath G, Bisaro DM. 2009. Geminivirus AL2 and L2 proteins suppress transcriptional gene silencing and cause genome-wide reductions in cytosine methylation. J Virol 83:5005–5013. https://doi.org/10.1128/JVI.01771-08.

7. Yang X, Xie Y, Raja P, Li S, Wolf JN, Shen Q, Bisaro DM, Zhou X. 2011. Suppression of methylation-mediated transcriptional gene silencing by βC1-SAHH protein interaction during geminivirus-betasatellite infection. PLoS Pathog 7:e1002329. https://doi.org/10.1371/journal.ppat.1002329.

8. Castillo-Gonzalez C, Liu X, Huang C, Zhao C, Ma Z, Hu T, Sun F, Zhou Y, Zhou X, Wang X-J, Zhang X. 2015. Geminivirus-encoded TrAP suppressor inhibits the histone methyltransferase SUVH4/KYP to counter host defense. Elife 4:e06671. https://doi.org/10.7554/eLife.06671.

9. Jackel JN, Buchmann RC, Singhal U, Bisaro DM. 2015. Analysis of geminivirus AL2 and L2 proteins reveals a novel AL2 silencing suppressor activity. J Virol 89:3176–3187. https://doi.org/10.1128/JVI.02625-14.

10. Law JA, Jacobsen SE. 2010. Establishing, maintaining, and modifying DNA methylation patterns in plants and animals. Nat Rev Genet 11:204–220. https://doi.org/10.1038/nrg2719.

11. Raja P, Wolf JN, Bisaro DM. 2010. RNA silencing directed against geminiviruses: post-transcriptional and epigenetic components. Biochim Biophys Acta 1799:337–351. https://doi.org/10.1016/j.bbagrm.2010.01.004.

12. Matzke MA, Mosher RA. 2014. RNA-directed DNA methylation: an epigenetic pathway of increasing complexity. Nat Rev Genet 15:394–408. https://doi.org/10.1038/nrg3683.

13. Fultz D, Choudury SG, Slotkin RK. 2015. Silencing of active transposable elements in plants. Curr Opin Plant Biol 27:67–76. https://doi.org/10.1016/j.pbi.2015.05.027.

14. Panda K, Slotkin RK. 2013. Proposed mechanism for the initiation of transposable element silencing by the RDR6-directed DNA methylation pathway. Plant Signal Behav 8:e25206. https://doi.org/10.4161/psb.25206.

15. Cuerda-Gil D, Slotkin RK. 2016. Non-canonical RNA-directed DNA methylation. Nat Plants 2:16163. https://doi.org/10.1038/nplants.2016.163.

16. Jackel JN, Storer JM, Coursey T, Bisaro DM. 2016. Arabidopsis RNA polymerases IV and V are required to establish H3K9 methylation, but not cytosine methylation, on geminivirus chromatin. J Virol 90:7529–7540. https://doi.org/10.1128/JVI.00656-16.

17. Jeske H. 2009. Geminiviruses. Curr Top Microbiol Immunol 331:185–226.

18. Hanley-Bowdoin L, Bejarano ER, Robertson D, Mansoor S. 2013. Geminiviruses: masters at redirecting and reprogramming plant processes. Nat Rev Microbiol 11:777–788. https://doi.org/10.1038/nrmicro3117.

19. Pilartz M, Jeske H. 1992. Abutilon mosaic virus double-stranded DNA is packed into minichromosomes. Virology 189:800–802. https://doi.org/10.1016/0042-6822(92)90610-2.

20. Pilartz M, Jeske H. 2003. Mapping of Abutilon mosaic geminivirus mini-

chromosomes. J Virol 77:10808–10818. https://doi.org/10.1128/JVI.77.20.10808-10818.2003.

21. Paprotka T, Deuschle K, Pilartz M, Jeske H. 2015. Form follows function in geminiviral minichromosome architecture. Virus Res 196:44–55. https://doi.org/10.1016/j.virusres.2014.11.004.

22. Raja P, Jackel JN, Li S, Heard IM, Bisaro DM. 2014. Arabidopsis double-stranded RNA binding protein DRB3 participates in methylation-mediated defense against geminiviruses. J Virol 88:2611–2622. https://doi.org/10.1128/JVI.02305-13.

23. Ceniceros-Ojeda EA, Rodriguez-Negrete EA, Rivera-Bustamante RF. 2016. Two populations of viral minichromosomes are present in a geminivirus-infected plant showing symptom remission (recovery). J Virol 90:3828–3838. https://doi.org/10.1128/JVI.02385-15.

24. Giresi PG, Kim J, McDaniell RM, Iyer VR, Lieb JD. 2007. FAIRE (formaldehyde-assisted isolation of regulatory elements) isolates active regulatory elements from human chromatin. Genome Res 17:877–885. https://doi.org/10.1101/gr.5533506.

25. Arbuckle JH, Kristie TM. 2014. Epigenetic repression of herpes simplex virus infection by the nucleosome remodeler CHD3. mBio 5:e01027-13. https://doi.org/10.1128/mBio.01027-13.

26. Omidbakhshfard MA, Winck FV, Arvidsson S, Riano-Pachon DM, Mueller-Roeber B. 2013. A step-by-step protocol for formaldehyde-assisted isolation of regulatory elements from Arabidopsis thaliana. J Int Plant Biol 56:527–538. https://doi.org/10.1111/jipb.12151.

27. Lister R, O'Malley RC, Tonti-Filippini J, Gregory BD, Berry CC, Millar AH, Ecker JR. 2008. Highly integrated single-base resolution maps of the epigenome in Arabidopsis. Cell 133:523–536. https://doi.org/10.1016/j.cell.2008.03.029.

28. Zhang Z, Chen H, Huang X, Xia R, Zhao Q, Lai J, Teng K, Li Y, Liang L, Du Q, Zhou X, Guo H, Xie Q. 2011. BSCTV C2 attenuates the degradation of SAMDC1 to suppress DNA methylation-mediated gene silencing in Arabidopsis. Plant Cell 23:273–288. https://doi.org/10.1105/tpc.110.081695.

29. Hormuzdi SG, Bisaro DM. 1995. Genetic analysis of beet curly top virus: examination of the roles of L2 and L3 genes in viral pathogenesis. Virology 206:1044–1054. https://doi.org/10.1006/viro.1995.1027.

30. Rushing AE, Sunter G, Gardiner WE, Dute RR, Bisaro DM. 1987. Ultrastructural aspects of tomato golden mosaic virus infection in tobacco. Phytopathology 77:1231–1236. https://doi.org/10.1094/Phyto-77-1231.

31. Bass HW, Nagar S, Hanley-Bowdoin L, Robertson D. 2000. Chromosome condensation induced by geminivirus infection of mature plant cells. J Cell Sci 113:1149–1160.

32. Mieczkowski J, Cook A, Bowman SK, Mueller B, Alver BH, Kundu S, Deaton AM, Urban JA, Larschan E, Park PJ, Kingston RE, Tolstorukov MY. 2016. MNase titration reveals differences between nucleosome occupancy and chromatin accessibility. Nat Commun 7:11485. https://doi.org/10.1038/ncomms11485.

33. Ebbs ML, Bartee L, Bender J. 2005. H3 lysine 9 methylation is maintained on a transcribed inverted repeat by combined action of SUVH6 and SUVH4 methyltransferases. Mol Cell Biol 25:10507–10515. https://doi.org/10.1128/MCB.25.23.10507-10515.2005.

34. Ebbs ML, Bender J. 2006. Locus-specific control of DNA methylation by the Arabidopsis SUVH5 histone methyltransferase. Plant Cell 18:1166–1176. https://doi.org/10.1105/tpc.106.041400.

35. Wierzbicki AT, Haag JR, Pikaard CS. 2008. Noncoding transcription by RNA polymerase IVb/PolV mediates transcriptional silencing of overlapping and adjacent genes. Cell 135:635–648. https://doi.org/10.1016/j.cell.2008.09.035.

36. Blevins T, Podicheti R, Mishra V, Marasco M, Wang J, Rusch D, Tang H, Pikaard CS. 2015. Identification of Pol IV and RDR2-dependent precursors of 24 nt siRNAs guiding de novo DNA methylation in Arabidopsis. Elife 4:e09591. https://doi.org/10.7554/eLife.09591.

37. Li S, Vandivier LE, Tu B, Gao L, Won SY, Li S, Zheng B, Gregory BD, Chen X. 2015. Detection of Pol IV/RDR2-dependent transcripts at the genome

scale in *Arabidopsis* reveals features and regulation of siRNA biogenesis. Genome Res 25:235–245. https://doi.org/10.1101/gr.182238.114.

38. Zhai J, Bischof S, Wang H, Feng S, Lee T-F, Teng C, Chen X, Park SY, Liu L, Gallego-Bartolome J, Liu W, Henderson IR, Meyers BC, Ausin I, Jacobsen SE. 2015. A one precursor one siRNA model for Pol IV-dependent siRNA biogenesis. Cell 163:445–455. https://doi.org/10.1016/j.cell.2015.09.032.

39. Vaillant I, Schubert I, Tourmente S, Mathieu O. 2006. MOM1 mediates DNA-methylation-independent silencing of repetitive sequences in *Arabidopsis*. EMBO Rep 7:1273–1278. https://doi.org/10.1038/sj.embor.7400791.

40. Sigman M, Slotkin RK. 2016. The first rule of plant transposable element silencing: location, location, location. Plant Cell 28:304–313. https://doi.org/10.1105/tpc.15.00869.

41. Nuthikattu S, McCue AD, Panda K, Fultz D, DeFraia C, Thomas EN, Slotkin RK. 2013. The initiation of epigenetic silencing of active transposable elements is triggered by RDR6 and 21-22 nucleotide small interfering RNAs. Plant Physiol 162:116–131. https://doi.org/10.1104/pp.113.216481.

42. Butterbach P, Verlaan MG, Dullemans A, Lohuis D, Visser RGF, Bai Y, Kormelink R. 2014. Tomato yellow leaf curl virus resistance by Ty-1 involves increased cytosine methylation of viral genomes and is compromised by cucumber mosaic virus infection. Proc Natl Acad Sci U S A 111:12942–12947. https://doi.org/10.1073/pnas.1400894111.

43. Du J, Johnson LM, Jacobsen SE, Patel DJ. 2015. DNA methylation pathways and their crosstalk with histone methylation. Nature Rev Mol Cell Biol 16:519–532. https://doi.org/10.1038/nrm4043.

44. Ascencio-Ibanez JT, Sozzani R, Lee TJ, Chu TM, Wolfinger RD, Cella R, Hanley-Bowdoin L. 2008. Global analysis of Arabidopsis gene expression uncovers a complex array of changes impacting pathogen response and cell cycle during geminivirus infection. Plant Physiol 148:436–454. https://doi.org/10.1104/pp.108.121038.

45. Monier K, Armas JCG, Etteldorf S, Ghazal P, Sullivan KF. 2000. Annexation of the interchromosomal space during viral infection. Nat Cell Biol 2:661–665. https://doi.org/10.1038/35023615.

46. Simpson-Holley M, Colgrove RC, Nalepa G, Harper JW, Knipe DM. 2005. Identification and functional evaluation of cellular and viral factors involved in alteration of nuclear architecture during herpes simplex virus 1 infection. J Virol 79:12840–12851. https://doi.org/10.1128/JVI.79.20.12840-12851.2005.

47. Palauqui J-C, Elmayan T, Pollien J-M, Vaucheret H. 1997. Systemic acquired silencing: transgene-specific post-transcriptional silencing is transmitted by grafting from silenced stocks to non-silenced scions. EMBO J 16:4738–4745. https://doi.org/10.1093/emboj/16.15.4738.

48. Ratcliff F, Harrison BD, Baulcombe DC. 1997. A similarity between viral defense and gene silencing in plants. Science 276:1558–1560. https://doi.org/10.1126/science.276.5318.1558.

49. Al-Kaff NS, Covey SN, Kreike MM, Page AM, Pinder R, Dale PJ. 1998. Transcriptional and posttranscriptional plant gene silencing in response to a pathogen. Science 279:2113–2115. https://doi.org/10.1126/science.279.5359.2113.

50. Guo HS, Ding SW. 2002. A viral protein inhibits the long range signaling activity of the gene silencing signal. EMBO J 21:398–407. https://doi.org/10.1093/emboj/21.3.398.

51. Molnar A, Melnyk CW, Bassett A, Hardcastle TJ, Dunn R, Baulcombe DC. 2010. Small silencing RNAs in plants are mobile and direct epigenetic

modification in recipient cells. Science 328:872–875. https://doi.org/10.1126/science.1187959.

52. Melnyk CW, Molnar A, Basset AR, Baulcombe DC. 2011. Mobile 24 nt small RNAs direct transcriptional gene silencing in the root meristems of *Arabidopsis thaliana*. Curr Biol 21:1678–1683. https://doi.org/10.1016/j.cub.2011.08.065.

53. Lewsey MG, Hardcastle TJ, Melnyk CW, Molnar A, Valli A, Urich MA, Nery JR, Baulcombe DC, Ecker JR. 2016. Mobile small RNAs regulate genome-wide DNA methylation. Proc Natl Acad Sci U S A 113:E801–E810. https://doi.org/10.1073/pnas.1515072113.

54. Teixeira FK, Heredia F, Sarazin A, Roudier F, Boccara M, Ciaudo C, Cruaud C, Poulain J, Berdasco M, Fraga MF, Voinnet O, Wincker P, Esteller M, Colot V. 2009. A role for RNAi in the selective correction of DNA methylation defects. Science 323:1600–1604. https://doi.org/10.1126/science.1165313.

55. Ito H, Gaubert H, Bucher E, Mirouze M, Vaillant I, Paszkowski J. 2011. An siRNA pathway prevents transgenerational retrotransposition in plants subjected to stress. Nature 472:115–119. https://doi.org/10.1038/nature09861.

56. Fultz D, Slotkin RK. 2017. Exogenous transposable elements circumvent identity-based silencing, permitting dissections of expression-dependent silencing. Plant Cell 29:360–376. https://doi.org/10.1105/tpc.16.00718.

57. Stroud H, Greenberg MVC, Feng S, Bernatavichute YV, Jacobsen SE. 2013. Comprehensive analysis of silencing mutants reveals complex regulation of the *Arabidopsis* methylome. Cell 152:352–364. https://doi.org/10.1016/j.cell.2012.10.054.

58. Han Y-F, Dou K, Ma Z-Y, Zhang S-W, Huang H-W, Li L, Cai T, Chen S, Zhu J-K, He X-J. 2014. SUVR2 is involved in transcriptional gene silencing by associating with SNF2-related chromatin remodeling proteins in *Arabidopsis*. Cell Res 24:1445–1465. https://doi.org/10.1038/cr.2014.156.

59. Groth M, Stroud H, Feng S, Greenberg MVC, Vashisht AA, Wohlschlegel JA, Jacobsen SE, Ausin I. 2014. SNF2 chromatin remodeler-family proteins FRG1 and -2 are required for RNA-directed DNA methylation. Proc Natl Acad Sci U S A 111:17666–17671. https://doi.org/10.1073/pnas.1420515111.

60. Pontes O, Li CF, Nunes PC, Haag J, Ream T, Vitins A, Jacobsen SE, Pikaard CS. 2006. The *Arabidopsis* chromatin-modifying nuclear siRNA pathway involves a nucleolar RNA processing center. Cell 126:79–92. https://doi.org/10.1016/j.cell.2006.05.031.

61. Shu H, Gruissem W, Hennig L. 2013. Measuring Arabidopsis chromatin accessibility using DNaseI-polymerase chain reaction and DNase1-Chip assays. Plant Physiol 162:1794–1801. https://doi.org/10.1104/pp.113.220400.

62. Wang Y, Qu J, Ji S, Wallace AJ, Wu J, Li Y, Gopalan V, Ding B. 2016. A land plant-specific transcription factor directly enhances transcription of a pathogenic non-coding RNA template by DNA-dependent RNA polymerase II. Plant Cell 28:1094–1107. https://doi.org/10.1105/tpc.16.00100.

63. Schmittgen TD, Livak KJ. 2008. Analyzing real-time PCR data by the comparative CT method. Nat Protoc 3:1101–1108. https://doi.org/10.1038/nprot.2008.73.

64. Gruntman E, Qi Y, Slotkin RK, Roeder T, Martienssen RA, Sachidanandam R. 2008. Kismeth: analyzer of plant methylation states through bisulfite sequencing. BMC Bioinformatics 9:371. https://doi.org/10.1186/1471-2105-9-371.